1   SARS-CoV-2 Mac1 is required for IFN antagonism and efficient virus replication in mice.

2

3   Yousef M. Alhammad[1*], Srivatsan Parthasarathy[1*], Roshan Ghimire[2*], Joseph J. O'Connor[1],
4   Catherine M. Kerr[1], Jessica J. Pfannenstiel[1], Debarati Chanda[2], Caden A. Miller[2], Robert L.
5   Unckless[1], Sonia Zuniga[3], Luis Enjuanes[3], Sunil More[2], Rudragouda Channappanavar[2#],
6   Anthony R. Fehr[1#]

7   [1]Department of Molecular Biosciences, University of Kansas, Lawrence, Kansas 66047, USA
8   [2]Department of Veterinary Pathobiology, Oklahoma State University, Stillwater, Oklahoma,
9   United States,
10   [3]National Center of Biotechnology (CNB-CSIC), Campus Universidad Autónoma de Madrid,
11   Madrid, Spain

12

13   [*]These authors contributed equally to this work

14

15   [#]Correspondence: arfehr@ku.edu; Tel.: +1- (785) 864-6626; rchanna@okstate.edu; Tel.: +1-
16   (405) 744-7224

17

18   Running title: SARS-CoV-2 Mac1 is an essential virulence factor

19

20   Keywords: Coronavirus, SARS-CoV-2, Non-Structural Proteins, Macrodomain, ADP-
21   ribosylation, Interferon, Cytokines, Inflammatory Monocytes, Innate Immunity

ABSTRACT

Several coronavirus (CoV) encoded proteins are being evaluated as targets for antiviral therapies for COVID-19. Included in this set of proteins is the conserved macrodomain, or Mac1, an ADP-ribosylhydrolase and ADP-ribose binding protein. Utilizing point mutant recombinant viruses, Mac1 was shown to be critical for both murine hepatitis virus (MHV) and severe acute respiratory syndrome (SARS)-CoV virulence. However, as a potential drug target, it is imperative to understand how a complete Mac1 deletion impacts the replication and pathogenesis of different CoVs. To this end, we created recombinant bacterial artificial chromosomes (BACs) containing complete Mac1 deletions (ΔMac1) in MHV, MERS-CoV, and SARS-CoV-2. While we were unable to recover infectious virus from MHV or MERS-CoV ΔMac1 BACs, SARS-CoV-2 ΔMac1 was readily recovered from BAC transfection, indicating a stark difference in the requirement for Mac1 between different CoVs. Furthermore, SARS-CoV-2 ΔMac1 replicated at or near wild-type levels in multiple cell lines susceptible to infection. However, in a mouse model of severe infection, ΔMac1 was quickly cleared causing minimal pathology without any morbidity. ΔMac1 SARS-CoV-2 induced increased levels of interferon (IFN) and interferon-stimulated gene (ISG) expression in cell culture and mice, indicating that Mac1 blocks IFN responses which may contribute to its attenuation. ΔMac1 infection also led to a stark reduction in inflammatory monocytes and neutrophils. These results demonstrate that Mac1 only minimally impacts SARS-CoV-2 replication, unlike MHV and MERS-CoV, but is required for SARS-CoV-2 pathogenesis and is a unique antiviral drug target.

SIGNIFICANCE

All CoVs, including SARS-CoV-2, encode for a conserved macrodomain (Mac1) that counters host ADP-ribosylation. Prior studies with SARS-CoV-1 and MHV found that Mac1 blocks IFN production and promotes CoV pathogenesis, which has prompted the development of SARS-CoV-2 Mac1 inhibitors. However, development of these compounds into antivirals requires that we understand how SARS-CoV-2 lacking Mac1 replicates and causes disease *in vitro* and *in vivo*. Here we found that SARS-CoV-2 containing a complete Mac1 deletion replicates normally in cell culture but induces an elevated IFN response, has reduced viral loads *in vivo*, and does not cause significant disease in mice. These results will provide a roadmap for testing Mac1 inhibitors, help identify Mac1 functions, and open additional avenues for coronavirus therapies.

2

INTRODUCTION

53

54 Coronaviruses (CoVs) belong to the family *coronaviridae* and possess a large, positive-sense
55 RNA genome. The subfamily *coronavirinae* is further subdivided into α, β, γ and δ-CoVs,
56 though only the α and β-CoVs include viruses that infect humans. Prior to the 21st century CoVs
57 were predominantly known to cause mild respiratory disease in humans (1). However, with the
58 emergence of SARS-CoV, MERS-CoV, and most recently SARS-CoV-2, it is now well-
59 established that CoVs are implicated in severe human respiratory conditions and are a serious
60 threat to human health.

61 *Co*rona*v*irus *i*nfectious *d*isease (COVID-19) caused by SARS-CoV-2 is responsible for the
62 pandemic that has resulted in over 6 million deaths worldwide (WHO). In cases of severe
63 COVID-19, SARS-CoV-2 induces a robust pro-inflammatory cytokine response, or cytokine
64 storm, in the host leading to the development of acute respiratory distress syndrome (ARDS) and
65 in some cases multiple organ pathologies (2). Introduction of SARS-CoV-2 mRNA vaccines
66 have drastically increased antiviral immunity and has reduced the fatality caused by SARS-CoV-
67 2 (CDC). However, many elderly or immunocompromised people have ineffective responses to
68 vaccines (3), and with the rate of emergence of new SARS-CoV-2 variants like Omicron (BA.2,
69 BA.4 and BA.5) there is an urgent need to identify novel antiviral drugs. Currently, a few
70 antiviral drugs such as Veklury (Remdesivir) (4, 5) and Lagevrio (molnupiravir) (5) both of
71 which target the CoV polymerase (nsp12); and Paxlovid (nirmatrelvir and ritonavir) (6), which
72 targets the main protease (nsp5), have been utilized in hospitals to treat COVID-19 patients
73 under adverse conditions. However, it remains important to identify novel drug targets to expand
74 the pool of anti-CoV therapies that will be needed to account for drug-resistance, provide
75 additional options for treatment, and better understand the replication processes of CoVs.

76 All CoVs encode a conserved set of 15-16 non-structural proteins that direct the formation of the
77 replication transcription complex (RTC) and carryout the process of RNA transcription and
78 replication, making these proteins important targets for antiviral therapies. While much progress
79 has been made in identifying the functions of many of the non-structural proteins, we still lack a
80 complete understanding of how these proteins contribute to RNA replication and evasion of the
81 host immune response. Non-structural protein 3 (nsp3) is the largest non-structural protein
82 encoded in the CoV genome and consists of several modular protein domains, such as the
83 papain-like protease (PLP) domain. Included in these domains of nsp3 are 3 tandem
84 macrodomains (Mac1, Mac2 and Mac3). Mac1 is conserved throughout all CoVs unlike Mac2
85 and Mac3 (7-12). Notably, homologs of Mac1 are also found in other viruses like alphaviruses,
86 hepatitis E virus, and rubella virus, suggesting it could play an important role in the replication of
87 a subset of positive-strand RNA viruses (13, 14). Structurally, macrodomains are characterized
88 by the presence of a conserved three-layered α/β/α fold. Biochemically, the conserved viral
89 macrodomain binds to ADP-ribose moieties with high affinity (15, 16) and in some cases can
90 hydrolyze the bond between ADP-ribose and proteins, reversing ADP-ribosylation, a common
91 post-translational modification (15, 17-20).

92 ADP-ribosylation is catalyzed by ADP-ribosyltransferases (ARTs/PARPs) using NAD^+ as the
93 substrate (21). ADP-ribose subunits can be added to proteins as single subunits in a process
94 termed mono-ADP-ribosylation (or MARylation) or as a polymer of ADP-ribose subunits
95 forming a chain in a process termed poly-ADP-ribosylation (or PARylation). Notably, several of
96 the MARylating PARPs are interferon stimulated genes (ISGs) and demonstrate antibacterial and

3

97   antiviral properties (22-25). These results highlight the importance of ADP-ribosylation as a
98   putative antiviral host response and viral macrodomains as an evolutionary adaptation by certain
99   viruses to counter this host response (17, 19, 20). Therefore, it is of interest to better understand
100 how viral macrodomains counter PARP activity and contribute towards viral infection and
101 pathogenesis.

102 The recent body of research has identified Mac1 as a viral factor necessary for CoV replication
103 and pathogenesis in multiple animal models of infection (18, 26). Most of these studies have
104 utilized a point mutant of Mac1 where a conserved asparagine residue (N1347 in MHV-JHM)
105 was mutated to an alanine. This mutation dramatically reduces the ability of Mac1 to hydrolyze
106 MAR from target proteins (16, 18, 27-29). The SARS-CoV-1 Mac1 asparagine-to-alanine mutant
107 virus (N1040A) had minimal to no impact on replication in transformed cells but was sensitive to
108 IFN pre-treatment and induced robust IFN and pro-inflammatory cytokine production and caused
109 minimal disease in mouse models of infection (18, 30). Similar results were seen with the
110 corresponding MHV Mac1 mutant virus (N1347A), though growth defects have been observed
111 in some cell types with these viruses (31-33). Importantly MHV-N1347A replication increased
112 upon PARP inhibition or knockdown of PARP12 or 14, while WT virus was unaffected.
113 Similarly, IFN induction following infection with MHV N1347A was nearly eliminated upon
114 PARP inhibition and in PARP14 knockout cells. These results demonstrate that Mac1 function
115 countered the action of PARP mediated ADP-ribosylation (32). Apart from N1347A, we found
116 that another unique mutation, D1329A, a residue which is critical for the ADP-binding activity
117 of macrodomains, replicated poorly in multiple cell types. Additionally, we were unable to
118 recover an MHV double mutant virus, D1329A/N1347A, indicating that Mac1 may be critical
119 for CoV replication. These results demonstrate that Mac1 has multiple functions that can
120 promote viral replication and block host interferon responses (33).

121 These combined studies have prompted several groups to begin screening for and developing
122 SARS-CoV-2 Mac1 inhibitors that could potentially be used therapeutically to treat patients
123 infected with SARS-CoV-2 or other emerging CoVs (34-41). However, before testing any of
124 these inhibitors for their antiviral activity, it is imperative to determine the role and functions of
125 Mac1 in SARS-CoV-2 replication, pathogenesis, and the host immune response. Here we have
126 created a complete SARS-CoV-2 Mac1 deletion virus and characterized its replication and
127 immune modulating properties. These results provide new insights into SARS-CoV-2 biology,
128 the innate immune response to infection, and will provide a roadmap for future testing of Mac1
129 inhibitors for antiviral activity.

130   **RESULTS**

131   **SARS-CoV-2 Mac1 deletion virus infectious virus was easily recovered while Mac1 deletion**
132   **viruses in other *β*-CoVs were not recovered.** We recently identified several Mac1 mutations in
133   murine hepatitis virus strain JHM (MHV-JHM) that were unrecoverable from a bacterial
134   artificial chromosome (BAC) based reverse genetic system (33). These results indicated that
135   Mac1 may be critical for MHV replication. As point mutations could result in toxic unfolded
136   proteins, we created an MHV-JHM Mac1 deletion BAC to confirm our prior results. As
137   expected, we were unable to recover infectious virus (Fig. S1A-B) from the Mac1 deletion BAC,
138   further indicating that Mac1 is critical for MHV-JHM replication. We next created a complete
139   deletion of Mac1 in MERS-CoV, and again we were unable to recover infectious virus,
140   indicating that Mac1 is also critical for MERS-CoV replication (Fig. S1A-B). We hypothesized
141   that Mac1 might be essential for the replication of all CoVs, so we engineered a Mac1 deletion
142   (*Δ*Mac1) into a SARS-CoV-2 BAC (Wuhan strain) to provide additional evidence for our
143   hypothesis. However, unlike MHV-JHM or MERS-CoV, this virus was easily recoverable (Fig.
144   S1A-B). This result indicates that there are stark differences in the requirement for Mac1
145   between SARS-CoV-2 and other *β*-CoVs.

146   **SARS-CoV-2 *Δ*Mac1 replicates like WT virus in most cell types.** Next, we assessed the ability
147   of SARS-CoV-2 *Δ*Mac1 to replicate in several cell types susceptible to SARS-CoV-2. In Vero
148   E6 cells *Δ*Mac1 replicated like WT virus cells at both low (Fig. 1A) and high (Fig. 1B)
149   multiplicity of infection (MOI), indicating that Mac1 is not required for general virus replication.
150   Vero E6 cells lack the ability to produce IFN-I, and MHV-JHM Mac1 mutant viruses are more
151   attenuated in cells that maintain the ability to produce IFN-I (32). Thus, we hypothesized that
152   SARS-CoV-2 *Δ*Mac1 may be attenuated in either A549-ACE2 (alveolar epithelial cells) or Calu-
153   3 cells (bronchial epithelial cells) that have a functional IFN system. *Δ*Mac1 replicated equally to
154   WT virus in A549-ACE2 cells (Fig. 1C), however there was a mild, ~2-3-fold reduction in
155   *Δ*Mac1 titers in Calu-3 cells compared to WT virus at both low (Fig. 2A-B) and high MOI (Fig.
156   2C-D). We further observed only mild, if any, reduction in viral N protein when analyzed by
157   immunoblotting and we observed roughly equal levels of both N protein and nsp3 staining by
158   confocal microscopy (Fig. 2E-F) in Calu-3 cells infected by WT and *Δ*Mac1. To evaluate the
159   relative fitness of *Δ*Mac1 compared to WT virus, we performed a competition experiment where
160   we co-infected Calu-3 cells with WT and *Δ*Mac1 at ratios of 1:1 and 1:9, respectively, and
161   followed these viruses over the course of 4 passages. Virus was collected at approximately 36
162   hpi after each passage to isolate virus during active replication, and not after peak replication has
163   been reached. To distinguish between WT and *Δ*Mac1 viruses, we used semi-quantitative RT-
164   PCR with primers set outside of Mac1 that produce different sized PCR products from each
165   virus. First, using BAC DNA, we found that the ratio of these bands correlated with the ratio of
166   input BAC (Fig. S2A-B), indicating that this method could faithfully define the relative
167   abundance of each virus following passaging. We found that after 4 rounds of passaging *Δ*Mac1
168   had not been outcompeted by WT virus as the ratios of these two viruses stayed relatively stable
169   over the entire experiment (Fig. S2C-D), though WT virus was starting to increase in abundance
170   in the 9:1 (*Δ*Mac1:WT) sample at passage 4. In total, these results indicate that *Δ*Mac1 generally
171   replicates like WT virus but has a mild replication defect in Calu-3 cells, though it has similar
172   fitness as WT virus in Calu-3 cells.

173 **SARS-CoV-2 *ΔMac1* is more sensitive to IFN-γ pre-treatment than WT virus.** We
174 previously found that IFN-β pretreatment more effectively reduced MHV Mac1 mutant virus
175 replication than WT virus replication in primary macrophages, likely due to the significant
176 upregulation of PARP enzymes (32). Thus, we tested the ability of IFN-β pre-treatment to
177 impede SARS-CoV-2 WT and *ΔMac1* infection in Calu-3 cells. We found that adding increasing
178 amounts of IFN-β to cells 18 hours before infection reduced *ΔMac1* replication to the same level
179 as WT virus in Calu-3 cells (Fig. 3A), indicating that SARS-CoV-2 *ΔMac1* is not more sensitive
180 to IFN-β than WT virus. We hypothesized that SARS-CoV-2 may be too sensitive to IFN-β to
181 distinguish any difference in the replication of WT and *ΔMac1* viruses. Therefore, we next used
182 IFN-γ, which induces a smaller number of ISGs and has reduced antiviral activity against SARS-
183 CoV-2 compared to IFN-β (42), but still induces the expression of PARP enzymes (Fig. S3)
184 (43). In contrast to results with IFN-β, pre-treatment of cells with increasing concentrations of
185 IFN-γ led to more robust inhibition of *ΔMac1* than WT virus when cells were infected at an MOI
186 of 0.1 and harvested at 48 hpi (Fig. 3B). The fold-difference in replication between WT and
187 *ΔMac1* ranged from 3-fold with no IFN-γ, which is consistent with results in Fig. 2, to ~20-fold
188 reduction in replication of *ΔMac1* compared to WT virus when cells were pretreated with 500
189 units of IFN-γ (Fig. 3B). These results demonstrate that IFN-γ pre-treatment of Calu-3 cells
190 more effectively impedes the replication of SARS-CoV-2 *ΔMac1* compared to WT virus.

191 **SARS-CoV-2 *ΔMac1* induces increased IFN and cytokine responses in cell culture.** Next, we
192 tested SARS-CoV-2 *ΔMac1* for its ability to induce IFNs and pro-inflammatory cytokines in cell
193 culture, as has previously been shown for Mac1 mutants in SARS-CoV and MHV (18, 32). We
194 found that in both Calu-3 (Fig. 4A) and A549-ACE2 cells *ΔMac1* infection induced greater
195 levels of both IFN-I and IFN-III transcript levels, and of ISGs such as ISG15 and CXCL-10 (Fig.
196 4B). However, the increase in IFN/ISG transcript levels, ~2-3 fold, is somewhat reduced
197 compared to those prior results with SARS-CoV-1 and MHV-JHM Mac1 mutant viruses (26,
198 32). This differences in IFN induction between WT and Mac1 deleted/mutant viruses between
199 different CoVs could be due to alterations in the functions or abundance of other CoV-encoded
200 IFN repressing proteins expressed by SARS-CoV-2.

201 **SARS-CoV-2 *ΔMac1* is highly attenuated in K18-ACE2 mice.** We next tested the ability of
202 SARS-CoV-2 WT and *ΔMac1* to cause disease in K18-ACE2 C57BL/6 mice, a lethal animal
203 model of SARS-CoV-2 infection. Following intranasally inoculation of 2.5×10^4 PFU WT SARS-
204 CoV-2, we observed 100% morbidity and mortality. In contrast, SARS-CoV-2 *ΔMac1* infection
205 did not cause any weight loss or lethality, indicating extreme attenuation (Fig. 5A-B). When
206 analyzing the infected lungs by hematoxylin and eosin staining, we noted significantly higher
207 levels of bronchointerstitial pneumonia, inflammation, and edema and fibrin in WT SARS-CoV-
208 2 infected lungs compared to *ΔMac1* virus infected lungs (Fig. 5C). We then compared the WT
209 and *ΔMac1* SARS-CoV-2 loads in infected lungs and found that by day 1 post-infection there
210 was a significant reduction in viral titers (Fig. 5E) and viral genomic RNA (gRNA) (Fig. 5F) of
211 ~ 1 log in the lungs of *ΔMac1* infected mice compared to WT SARS-Cov-2 infected lungs. The
212 difference in viral load between WT and *ΔMac1* increased to 2.5 logs by day 3, and by day 7
213 *ΔMac1* was effectively cleared from the lungs while WT virus was still present at about 10^5 PFU
214 in the lung (Fig. 5E-F). In contrast, viral loads in the brain were very low until after day 3 post-
215 infection, though WT virus was present at low levels in most mice by day 7, whereas *ΔMac1*
216 titers were below the detection limit at all days tested. (Fig. S4A). Further, there was no
217 significant difference in brain pathology between WT and *ΔMac1* infected mice (Fig. S4B),

6

218   indicating that brain infection and pathology did not significantly contribute to the weight loss
219   and mortality of WT virus infected mice.

220   **SARS-CoV-2 ΔMac1 induces a robust innate immune response in the lungs of K18-ACE2**
221   **mice.** The rapid clearance of ΔMac1 in the lungs of infected mice and prior results with Mac1
222   SARS-CoV mutant viruses (18) suggested that ΔMac1 would induce a strong innate immune
223   response in mice. To test this possibility, we measured the transcripts of a small panel of IFN and
224   ISGs for their expression following infection of WT and ΔMac1 at 1 day post infection (Fig.
225   6A). IFN-β and IFN-λ were upregulated by more than 10-fold in ΔMac1 infected lungs, while
226   IFN-γ was not detected. We also observed a ~2-3-fold increase in several ISGs, such as OAS,
227   ISG15, CXCL10, IL-6, PARP12, and PARP14. These results suggest that the attenuation of
228   ΔMac1 virus could, at least in part, be due to a robust IFN response at the early stages of
229   infection. To get a global view of all the transcriptional changes occurring in the absence of
230   Mac1, we performed RNAseq of whole lung samples collected at day 1 post-infection.
231   Differentially expressed genes were define as having at least 1.5-fold increased expression in
232   either WT or ΔMac1 infected lungs with an adjusted p value of <0.05. In total, we found 645
233   genes were increased following infection with ΔMac1, and another 230 were increased following
234   WT infection, including viral gRNA, for a total of 875 differentially regulated genes (Fig. 6B).
235   We then performed a gene ontology analysis, and found that genes related to immunity, innate
236   immunity, and antiviral defense were the pathways that were most significantly upregulated in
237   ΔMac1 infected lungs (Fig. 6C). In addition, genes in the categories of adaptive immunity,
238   ubiquitin conjugation, inflammatory responses, peptide transport, cytolysis, and apoptosis were
239   also significantly upregulated in ΔMac1 infected lungs (Fig. 6C). We then looked at the
240   individual expression of a panel of ISGs and found that most ISGs were increased between 2 and
241   4-fold in ΔMac1 when compared to WT virus infection, while IFN-β and IFN-λ were increased
242   more than 10-fold (Fig. 6D, Fig. S5). In total, we have found that Mac1 is required for SARS-
243   CoV-2 to block the innate immune response during SARS-CoV-2 infection in mice.

244   **SARS-CoV-2 ΔMac1 infection results in reduced myeloid cell accumulation in the lungs.**
245   Next, we assessed the impact of WT and ΔMac1 virus infection on the recruitment of innate
246   immune cells, specifically inflammatory monocytes and neutrophils, into the lung that might
247   contribute differential lung inflammation and disease severity. Inflammatory monocytes were
248   found to contribute to disease severity in SARS-CoV-1 and MERS-CoV infected mice by
249   promoting the production of TNFα and increased T cell apoptosis (44, 45). Previously, IFN-I
250   was shown to enhance inflammatory monocyte accumulation in the lung, though this was due to
251   IFN-I production in the later stages of SARS-CoV-1 replication (44). However, earlier
252   exogenous addition of IFN-I reduced inflammatory monocyte infiltration following MERS-CoV
253   infection was shown to reduce the number of inflammatory monocytes (45). Thus, we
254   hypothesized that the early IFN-I and IFN-III induction by ΔMac1 would result in fewer
255   infiltrating inflammatory immune cells. Following infection with ΔMac1, we observed a
256   substantial reduction in both the percentage and total number of inflammatory monocytes at both
257   3 and 7 days after infection (Fig. 7A), which could also play a role in the attenuation of the
258   disease severity. Neutrophils were slightly increased in percentage in ΔMac1 infected lungs at
259   day 3 but had similar total numbers when compared to WT virus infection (Fig. 7B). However,
260   by day 7 there was a significant reduction in the total number of neutrophils in ΔMac1 infected
261   lungs (Fig. 7B).

262 Overall, our results indicate that the absence of Mac1 promotes a strong IFN response with a
263 reduction in inflammatory cell types that may both play a role in reducing viral loads and
264 preventing disease following infection.

265 **DISCUSSION**

266 The COVID-19 pandemic caused by SARS-CoV-2, has fueled a new interest in the development
267 of inhibitors targeting viral gene products that block viral replication and pathogenesis, to be
268 used therapeutically to treat patients with COVID-19. This includes the $577 million-dollar
269 Antiviral Drug Development Award (AVIDD) initiated by the NIH in 2021. Thus far, antivirals
270 targeting the viral polymerase (nsp12) and protease (nsp5) have been approved for clinical use
271 (4-6), however a much larger anti-CoV drug portfolio is clearly needed to target SARS-CoV-2
272 and effectively respond to novel CoV outbreaks in the future. One of the CoV-encoded proteins
273 that has received increased attention as a potential drug target is the conserved macrodomain,
274 now called Mac1 (46). Multiple groups have initiated drug development programs targeting
275 Mac1, all utilizing biochemical assays that can be used to screen for compounds that inhibit
276 either Mac1-ADP-ribose binding or Mac1 ADP-ribosylhydrolase activity (34-41). Currently, the
277 top Mac1 inhibitors identified to date have IC_{50} values in these biochemical assays ranging from
278 ~0.5-10 μM. However, none of these compounds have been tested for their ability to inhibit virus
279 replication or pathogenesis in cell culture or in mice. While the current body of literature
280 indicates that Mac1 is important for the replication and pathogenesis of MHV and SARS-CoV-1
281 in mice (18, 26, 31), no study has yet evaluated how Mac1 impacts the replication of SARS-
282 CoV-2, which is critical for the ability to interpret inhibitor studies.

283 Prior results in our lab had indicated that Mac1 is critical for the replication of MHV-JHM, as at
284 least two Mac1 mutant recombinant BACs failed to produce infectious virus (33). However, one
285 of these mutations, G1439V, did replicate after acquiring a second site mutation in the residue
286 immediately preceding it, A1438T. To confirm these results, we created a complete deletion of
287 Mac1 in the MHV-JHM BAC and again found that we could not recover infectious virus (Fig.
288 S1A-B). We hypothesized that perhaps a Mac1 deletion may be detrimental across CoVs, so we
289 then created MERS-CoV and SARS-CoV-2 ΔMac1 recombinant BACs. Surprisingly, we were
290 unable to recover infectious virus from the MERS-CoV ΔMac1 BAC but easily recovered
291 infectious SARS-CoV-2 ΔMac1 (Fig. S1A-B). While we haven't tested a Mac1 deletion in
292 SARS-CoV-1, the near WT replication of the same G-V mutation in MHV described above
293 indicates that Mac1 is likely non-essential for SARS-CoV-1 as well (18). This near absolute
294 requirement for Mac1 in some CoV species but not in others was surprising, but not without
295 precedent. For instance, a recombinant virus with an E protein deletion was viable with only a
296 mild replication defect in SARS-CoV-1 (47), but an E protein deletion in MERS-CoV was
297 unrecoverable unless the virus was propagated on E protein expressing cells (48). Nsp14 ExoN
298 mutations are lethal in MERS-CoV and SARS-CoV-2 but are viable in MHV and SARS-CoV-1
299 (49). Finally, MHV nsp15 mutant viruses grow very poorly in IFN-competent macrophages (50,
300 51), while similar mutations in MERS-CoV replicate normally in IFN-competent cells (52). In
301 the cases of E protein and nsp15 the viruses that replicate normally in the absence of these
302 proteins have additional accessory proteins that have overlapping or redundant functions. For
303 instance, the 4a and 4b MERS-CoV proteins were found to have redundant functions with nsp15
304 in blocking the innate immune response to infection (52). We hypothesize that the
305 Sarbecoviruses may have evolved unique accessory proteins or other domains in the non-
306 structural proteins that have redundant functions with Mac1 in promoting viral replication.

8

307 Efforts to identify these proteins with redundant function are ongoing. Regardless, we and others
308 have found that Mac1 is critical for CoVs to replicate efficiently and cause disease in all animal
309 models of infection that have been tested (Fig. 5) (18, 26, 31).

310 Here we found that there was no defect in the replication of ΔMac1 in Vero E6 and A549 cells
311 and only a modest defect in Calu-3 cells. Given these results, along with modularity of the
312 various domains of nsp3, it is highly unlikely that the complete deletion of Mac1 had a
313 significant effect on the overall structure of nsp3. Despite the lack of a large replication defect of
314 ΔMac1 under normal growth conditions, we found that ΔMac1 had a >1 log defect in IFN-γ, but
315 not IFN-β treated Calu-3 cells (Fig. 5). IFN-γ induces a small number of ISGs compared to IFN-
316 β (43), and we hypothesized that while the PARP enzymes that inhibit Mac1 mutant MHV are
317 upregulated by both types of IFN, other more potent anti-SARS-CoV-2 ISGs are only
318 upregulated by IFN-β, or at least upregulated to a much higher level by IFN-β. We hypothesized
319 that these ISGs might limit viral entry, mitigating the effect of PARP enzymes to specifically
320 target the Mac1 mutant virus during later stages of the viral lifecycle. It will be of interest to
321 identify the specific PARP or PARPs that inhibit ΔMac1 following IFN-γ treatment and the
322 ADP-ribosylated target(s) that contribute to this inhibition. The ability to specifically reduce
323 ΔMac1 replication with IFN-γ could have important implications for Mac1 inhibitor testing.
324 Replication assays could be developed to assess the ability of the Mac1 inhibitors to reduce virus
325 replication in the absence and presence of IFN-γ to show that the inhibitors are indeed
326 specifically targeting Mac1. It may also be of interest to test the replication of ΔMac1 under
327 conditions of cell stress, such as ER stress or following activation of stress granules, as PARP
328 activity is known to be increased under stress conditions (53, 54).

329 Similar to SARS-CoV-1, we found that SARS-CoV-2 ΔMac1 induces a robust innate immune
330 response both in cell culture and in mice (Figs. 4,6), further confirming that Mac1 is one of the
331 many potent IFN repressing proteins expressed by CoVs. This innate immune response occurred
332 within one day of infection, and likely before peak replication of the virus. Whole lung RNAseq
333 data identified over 100 genes involved in immunity to virus infection, demonstrating the breadth
334 of the immune response that is triggered following ΔMac1 infection (Fig. 6B-D). We
335 hypothesize that this response at least partially protects mice from disease. We have previously
336 shown that the Mac1 mutant virus, N1347A, causes increased lethality and weight loss in IFNAR
337 knockout mice, and that providing exogenous IFN prior to peak viral replication is highly
338 protective in multiple animal models of CoV infection and protection is mediated by a
339 combination of increasing the abundance of antiviral ISGs, reducing the number of pro-
340 inflammatory monocytes, and increasing adaptive immunity (32, 44, 45). COVID-19 patients
341 with mutations in IFN related genes or that produce antibodies that target IFN have worse
342 outcomes than the general population, demonstrating the importance of IFN in protection from
343 severe COVID-19 (55-57). However, it remains unclear how an early IFN response from a virus
344 contributes to the protection of mice, and potentially humans, from disease. Some important
345 questions include: How is the IFN induced? Is it through MDA5, RIG-I, or other sensors? Which
346 cell type is the major IFN source from, epithelial or plasmacytoid dendritic cells or myeloid
347 cells? If it's coming from epithelial cells, which type of epithelial cell; nasal, bronchial, or
348 alveolar? Also, are both IFN-I and IFN-III important for protection, or is one of them sufficient?
349 Finally, how do these IFNs shape the overall innate and adaptive immune response? The answers
350 to these and other questions could have important implications for developing vaccines or

9

351   therapeutics that might stimulate better and longer lasting immunity and reduce incidence of
352   SARS-CoV-2 spread and disease in vulnerable populations.

353   **METHODS**

354   **Cell culture and reagents.** Vero E6, Huh-7, Baby Hamster Kidney cells expressing the mouse
355   virus receptor CEACAM1 (BHK-MVR) (gifts from Stanley Perlman, University of Iowa), and
356   A549-ACE2 cells (a gift from Susan Weiss, University of Pennsylvania), were grown in
357   Dulbecco's modified Eagle medium (DMEM) supplemented with 10% fetal bovine serum
358   (FBS). Calu-3 cells (ATCC) were grown in MEM supplemented with 20% FBS. Human IFN-β
359   and IFN-γ were purchased from R&D Systems. Cells were transfected with either Polyjet
360   (Amgen) or Lipofectamine 3000 (Fisher Scientific) per the instructions of the manufacturers.

361   **Mice.** Pathogen-free K18-ACE2 C57BL/6 mice were purchased from Jackson Laboratories.
362   Mice were bred and maintained in the animal resources facility at the Oklahoma State
363   University. Animal studies were approved by the University of Oklahoma State Institutional
364   Animal Care and Use Committee (IACUC) and met stipulations of the *Guide for the Care and*
365   *Use of Laboratory Animals.*

366   **Generation of recombinant pBAC-SARS-CoV-2, pBAC-MERS-CoV, and pBAC-JHMV**
367   **constructs.** All recombinant pBAC constructs were created using Red recombination (58) with
368   several previously described CoV bacterial artificial chromosomes (BACs). These include the
369   WT-SARS-CoV-2 BAC based off the Wuhan-Hu-1 isolate provided by Sonia Zuñiga, Li Wang,
370   Isabel Sola and Luis Enjuanes (CNB-CSIC, Madrid, Spain) (59), a MERS-CoV BAC based of
371   the EMC isolate (48), and an MHV BAC based on the JHMV isolate (26). All constructs were
372   engineered using a Kan$^{\text{r}}$-I-SceI marker cassette for dual positive and negative selection as
373   previously described (see primers in Table S1) (60). Both forward and reverse primers were
374   designed to include a 40bp region upstream of Mac1 to facilitate the deletion of Mac1 by
375   recombination (Table S1). Final BAC DNA constructs were confirmed by restriction enzyme
376   digestion, PCR, and direct sequencing for the identification of correct clones.

377   **Reconstitution of recombinant pBAC-SARS-CoV-2-derived virus.** All work with SARS-
378   CoV-2 and MERS-CoV was conducted in either the University of Kansas or the Oklahoma State
379   University EHS-approved BSL-3 facilities. To generate SARS-CoV-2 or MERS-CoV viruses,
380   approximately 5×10^5 Huh-7 cells were transfected with 2 μg of purified BAC DNA using
381   Lipofectamine 3000 (Fisher Scientific) as a transfection reagent. SARS-CoV-2 generated from
382   these transfections (p0) was then passaged in Vero E6 cells to great viral stocks (p1). All p1
383   stocks were again sequenced to confirm that they retained the correct Mac1 deletion and to
384   ensure the furin cleavage site had not been lost (for primers see Table S2). To generate MHV-
385   JHM and MERS-CoV virus, approximately 5×10^5 BHK-MVR cells were transfected with 1 μg
386   of purified BAC DNA using PolyJet™ Transfection Reagent (SignaGen). In the case of MHV-
387   JHM, an additional 1 μg of N protein-expressing plasmid was co-transfected with genomic BAC
388   DNA.

389   **Virus infection.** Vero-E6, A549-ACE2, or Calu-3 cells were infected at the indicated MOIs. For
390   Calu-3 cells, trypsin-TPCK (1 μg/ml) was added to the medium at the time of infection. All
391   infections included a 1-hour adsorption phase, except for Calu-3 cells where the adsorption phase
392   was increased to 2 hrs. Infected cells and supernatants were collected at indicated time points and
393   titers were determined on Vero E6 cells. For IFN pre-treatment experiments, human IFN-β and

10

394 IFN-γ were added to Calu-3 cells 18-20 hours prior to infection and were maintained in the
395 culture media throughout the infection. For animal infections, 12-16-week-old K18-ACE2
396 C57BL/6 female mice were lightly anesthetized using isoflurane and were intranasally infected
397 with 2.5×10^4 PFU in 50 μl DMEM. To obtain tissue for virus titers, mice were euthanized at
398 different days post challenge, lungs or brains were removed and homogenized in phosphate
399 buffered saline (PBS) and titers were determined on Vero E6 cells.

400 **Immunoblotting.** Total cell extracts were lysed in sample buffer containing SDS, protease and
401 phosphatase inhibitors (Roche), β-mercaptoethanol, and a universal nuclease (Fisher Scientific).
402 Proteins were resolved on an SDS polyacrylamide gel, transferred to a polyvinylidene difluoride
403 (PVDF) membrane, hybridized with a primary antibody, reacted with an infrared (IR) dye-
404 conjugated secondary antibody, visualized using a Li-COR Odyssey Imager (Li-COR), and
405 analyzed using Image Studio software. Primary antibodies used for immunoblotting included
406 anti-SARS-CoV-2 N (SinoBiological 40143-R001) and GAPDH (Millipore-Sigma G8795)
407 monoclonal antibodies. Secondary IR antibodies were purchased from Li-COR.

408 **Confocal Immunofluorescence.** Calu-3 cells were cultured with approximately 1.4×10^5 cells
409 per well in 8-well, removable chamber slides (ibidi 80841) and infected with SARS-CoV-2 at an
410 MOI of 1 PFU/cell. At 24 hpi, monolayers were fixed for 20 minutes with ice cold methanol then
411 10 minutes with 2% paraformaldehyde in HBSS + 0.01% Sucrose (HBSS/Su). Permeabilization
412 with 0.1% Saponin in HBSS/Su was then performed, followed by overnight blocking at 4°C
413 using 3% goat serum in HBSS/Su + Saponin. Primary antibody incubation was conducted for 3
414 hours at room temperature (1:2,000 α-N protein, Sino Biological 40143-R001; 1:500 α-nsp3,
415 abcam ab283958) followed by a 1 hour, room temperature secondary antibody incubation (1:200
416 AlexaFluor 555 Goat α-rabbit, Invitrogen A32732). Nuclear stain with 300nM DAPI was
417 performed at room temperature for 30 minutes followed by mounting in Vectashield Vibrance
418 Mounting Medium (Vector Labs H-1700) and storage at 4°C. Images were acquired using an
419 Olympus FV1000 laser-scanning confocal microscope equipped with Fluoview software. Images
420 were z-projected using maximum intensity.

421 **Semi-quantitative PCR analysis.** BAC DNA or infection-derived cDNA was PCR amplified by
422 primers that bind outside of the Mac1 coding sequence. PCR products were analyzed by gel
423 electrophoresis using a LICOR M imager and bands were quantified using Image Studio
424 software and the relative intensity of each band was determined by adding the overall intensity of
425 both bands together and then diving the intensity of each individual band by the total intensity.

426 **Real-time quantitative PCR (RT-qPCR) analysis.** RNA was isolated from cells using Trizol
427 (Invitrogen). Lungs from K18-ACE2 C57BL/6 mice infected with virus were collected at
428 indicated time points and were homogenized in Trizol (Invitrogen) and RNA was isolated using
429 manufacturer's instructions. cDNA was prepared using MMLV-reverse transcriptase per the
430 manufacturer's instructions (Thermo Fisher Scientific). qPCR was performed using PowerUp
431 SYBR green master mix (Applied Biosystems) and primers listed in Table S3. Cycle threshold
432 (CT) values were normalized to hypoxanthine phosphoribosyltransferase (HPRT) levels by using
433 the ΔCt method.

434 **RNAseq.** RNA was isolated from K18-ACE2 mice as described above. Library preparation was
435 performed by the University of Kansas Genome Sequencing core facility, using the NEB Next
436 RNA Library kit (NEB) with indexing. RNA-seq was performed using an Illumina NextSeq2000
437 high-output system with a paired-end reads of 50□bp each. RNAseq data quality was checked

11

438 using FastQC analysis pipeline. Samples had a minimum of 16 million reads and a mean quality
439 score (PF) >33. The mouse (C57BL6) transcriptome reference sequence
440 (GCF_000001635.27_GRCm39) and SARS-CoV-2 genome (Accession number - NC_045512.2)
441 were downloaded from NCBI genome collections and appended into a single sequence and used
442 as the reference sequence. RNAseq reads were mapped to the indexed reference sequence using
443 kallisto v0.44.0. Transcripts per kilobase per million mapped reads (TPM) and read counts per
444 transcript were extracted from the kallisto output. TPM values and read counts for all transcripts
445 from each gene were summed to obtain gene-level expression estimates, and the counts per gene
446 were then rounded to the nearest integer. For a given sample, we only considered genes with at
447 least 50 mapped reads total across all replicates from the samples. DESeq2 was used to identify
448 DEGs between the SARS-CoV-2 WT and ΔMac1 infected samples using simply "treatment" as a
449 factor. DEGs were identified based on the false-discovery rate corrected P-value (P_{ADJ}) and $\log_2$-
450 fold-change of ($\log_2$FC) between the samples. Genes were considered upregulated in a SARS-
451 CoV-2-infected sample if $P_{ADJ} < 0.05$ and $\log_2$FC > 0.6, which is nearly equivalent to a 1.5-fold
452 increase. Similarly, genes were considered downregulated if $P_{ADJ} < 0.05$ and $\log_2$FC < -0.6, or a
453 1.5-fold decrease. DEGs were subjected to gene ontology analysis using the Database for
454 Annotation, Visualization and Integrated Discovery (DAVID: https://david.ncifcrf.gov/). Gene
455 lists were analyzed for biological processes that were significantly enriched with P < 0.05 and
456 displayed as a clustered bar graph.

457 **Lung cell preparation and flow cytometry:** For phenotypic analyses of lung infiltrating
458 immune cells, lungs collected at different days post-infection, PBS perfused lungs (left lobe were
459 cut into small pieces, treated with collagenase-D and DNAse1 for 30 minutes at room
460 temperature, followed by homogenization of lung pieces using a 3ml syringe plunger
461 flang/thumb rest. Homogenized cells were passed through 70μM strainer to obtain single cell
462 suspension. Isolated single cell suspension was surface immunolabelled for neutrophil ($CD45^+$
463 $CD11b^+$ $Ly6G^{hi}$) and inflammatory monocyte ($CD45^+$ $CD11b^+$ $Ly6c^{hi}$) markers by flow
464 cytometry. For cell surface staining, lung cells were labelled with the following fluorochrome-
465 conjugated monoclonal antibodies: PECy7 α-CD45 (clone: 30-F11); FITC α-Ly6G (clone: 1A8);
466 PE/PerCp-Cy5.5 α-Ly6C (clone: HK1.4); V450 α-CD11b (clone: M1/70); APC α-F4/80 (clone:
467 BM8) (all procured from Biolegend). A detailed cell surface and intracellular immunolabelling
468 protocol for flow cytometry studies are described in our recent publication (61). All
469 fluorochrome-conjugated antibodies were used at a final concentration of 1:200 (antibody: FACS
470 buffer), except for FITC labeled antibodies used at 1:100 concentration.

471 **Histopathology.** The lung lobes were perfused and placed in 10% of formalin. Brain samples
472 were fixed in 10% formalin. The lung lobes and brain were then processed for hematoxylin and
473 eosin (H & E). The lung lesions were blindly scored by an American College of Veterinary
474 Pathology Board-certified pathologist. The lesions were scored on a scale of 0-10% (score 1),
475 10-40% (score 2), 40-70% (score 3) and >70% (score 4) and cumulative scores were obtained for
476 each mouse. The lesions scored were bronchiointerstitial pneumonia, peribronchial
477 inflammation, edema/fibrin, necrosis, and perivascular inflammation.

478 **Statistics.** A Student's *t* test was used to analyze differences in mean values between groups. All
479 results are expressed as means ± standard errors of the means (SEM). Differences in survival
480 were calculated using a Kaplan-Meier log-rank test. P values of ≤0.05 were considered
481 statistically significant (*, P≤0.05; **, P≤0.01; ***, P≤0.001; ****, P ≤0.0001; n.s., not
482 significant).

12

Data and materials availability. All the RNAseq reads data are deposited in NCBI under the BioProject ID PRJNA928501 and BioSample ID SAMN32942656 and SAMN32942675 and will be made public upon publication or August 31st 2023, whichever comes first.

Author contributions:
Conceptualization: YMA, SP, RC, ARF
Methodology: YMA, SP, RG, JJOC, CMK, JJP, RLU, SZ, LE, SM, RC, ARF
Investigation: YMA, SP, RG, JJOC, CMK, JJP, DC, CAM, SM, RC, ARF
Visualization: YMA, SP, RG, JJOC, CMK, JJP, SM, RC, ARF
Supervision: RC, ARF
Writing—original draft: ARF, YA, RC, SP
Writing—review & editing: ARF, RC, SP, RLU, SZ, LE

Competing interests: The University of Kansas-Lawrence has filed a patent application relating to coronavirus live-attenuated vaccines which lists A.R.F and R.C. as co-inventors.

REFERENCES

1. Y. Wang, M. Grunewald, S. Perlman, Coronaviruses: An Updated Overview of Their Replication and Pathogenesis. *Methods Mol Biol* **2203**, 1-29 (2020).

2. D. Blanco-Melo *et al.*, Imbalanced Host Response to SARS-CoV-2 Drives Development of COVID-19. *Cell* **181**, 1036-1045 e1039 (2020).

3. E. P. K. Parker *et al.*, Response to additional COVID-19 vaccine doses in people who are immunocompromised: a rapid review. *Lancet Glob Health* **10**, e326-e328 (2022).

4. J. H. Beigel, K. M. Tomashek, L. E. Dodd, Remdesivir for the Treatment of Covid-19 - Preliminary Report. Reply. *N Engl J Med* **383**, 994 (2020).

5. A. Wahl *et al.*, SARS-CoV-2 infection is effectively treated and prevented by EIDD-2801. *Nature* **591**, 451-457 (2021).

6. I. Gentile *et al.*, Nirmatrelvir/Ritonavir and Molnupiravir in the Treatment of Mild/Moderate COVID-19: Results of a Real-Life Study. *Vaccines (Basel)* **10** (2022).

7. A. Chatterjee *et al.*, Nuclear magnetic resonance structure shows that the severe acute respiratory syndrome coronavirus-unique domain contains a macrodomain fold. *J Virol* **83**, 1823-1836 (2009).

8. M. A. Johnson, A. Chatterjee, B. W. Neuman, K. Wuthrich, SARS coronavirus unique domain: three-domain molecular architecture in solution and RNA binding. *J Mol Biol* **400**, 724-742 (2010).

9. Y. Kusov, J. Tan, E. Alvarez, L. Enjuanes, R. Hilgenfeld, A G-quadruplex-binding macrodomain within the "SARS-unique domain" is essential for the activity of the SARS-coronavirus replication-transcription complex. *Virology* **484**, 313-322 (2015).

10. S. Srinivasan *et al.*, Structural Genomics of SARS-CoV-2 Indicates Evolutionary Conserved Functional Regions of Viral Proteins. *Viruses* **12** (2020).

11. J. Tan *et al.*, The "SARS-unique domain" (SUD) of SARS coronavirus is an oligo(G)-binding protein. *Biochem Biophys Res Commun* **364**, 877-882 (2007).

12. J. Tan *et al.*, The SARS-unique domain (SUD) of SARS coronavirus contains two macrodomains that bind G-quadruplexes. *PLoS Pathog* **5**, e1000428 (2009).

13. G. I. Makrynitsa *et al.*, Conformational plasticity of the VEEV macro domain is important for binding of ADP-ribose. *J Struct Biol* **206**, 119-127 (2019).

14. H. Malet *et al.*, The crystal structures of Chikungunya and Venezuelan equine encephalitis virus nsP3 macro domains define a conserved adenosine binding pocket. *J Virol* **83**, 6534-6545 (2009).

15. Y. M. O. Alhammad *et al.*, The SARS-CoV-2 Conserved Macrodomain Is a Mono-ADP-Ribosylhydrolase. *J Virol* **95** (2021).

16. M. P. Egloff *et al.*, Structural and functional basis for ADP-ribose and poly(ADP-ribose) binding by viral macro domains. *J Virol* **80**, 8493-8502 (2006).

17. L. Eckei *et al.*, The conserved macrodomains of the non-structural proteins of Chikungunya virus and other pathogenic positive strand RNA viruses function as mono-ADP-ribosylhydrolases. *Sci Rep* **7**, 41746 (2017).

18. A. R. Fehr *et al.*, The Conserved Coronavirus Macrodomain Promotes Virulence and Suppresses the Innate Immune Response during Severe Acute Respiratory Syndrome Coronavirus Infection. *mBio* **7** (2016).

19. C. Li *et al.*, Viral Macro Domains Reverse Protein ADP-Ribosylation. *J Virol* **90**, 8478-8486 (2016).

14

20. J. G. M. Rack *et al.*, Viral macrodomains: a structural and evolutionary assessment of the pharmacological potential. *Open Biol* **10**, 200237 (2020).

21. B. Luscher *et al.*, ADP-ribosyltransferases, an update on function and nomenclature. *FEBS J* 10.1111/febs.16142 (2021).

22. G. Caprara *et al.*, PARP14 Controls the Nuclear Accumulation of a Subset of Type I IFN-Inducible Proteins. *J Immunol* **200**, 2439-2454 (2018).

23. A. R. Fehr *et al.*, The impact of PARPs and ADP-ribosylation on inflammation and host-pathogen interactions. *Genes Dev* **34**, 341-359 (2020).

24. L. Li *et al.*, PARP12 suppresses Zika virus infection through PARP-dependent degradation of NS1 and NS3 viral proteins. *Sci Signal* **11** (2018).

25. S. Parthasarathy, A. R. Fehr, PARP14: A key ADP-ribosylating protein in host-virus interactions? *PLoS Pathog* **18**, e1010535 (2022).

26. A. R. Fehr *et al.*, The nsp3 macrodomain promotes virulence in mice with coronavirus-induced encephalitis. *J Virol* **89**, 1523-1536 (2015).

27. G. Jankevicius *et al.*, A family of macrodomain proteins reverses cellular mono-ADP-ribosylation. *Nat Struct Mol Biol* **20**, 508-514 (2013).

28. A. Putics, W. Filipowicz, J. Hall, A. E. Gorbalenya, J. Ziebuhr, ADP-ribose-1"-monophosphatase: a conserved coronavirus enzyme that is dispensable for viral replication in tissue culture. *J Virol* **79**, 12721-12731 (2005).

29. L. C. Russo *et al.*, The SARS-CoV-2 Nsp3 macrodomain reverses PARP9/DTX3L-dependent ADP-ribosylation induced by interferon signaling. *J Biol Chem* **297**, 101041 (2021).

30. T. Kuri *et al.*, The ADP-ribose-1"-monophosphatase domains of severe acute respiratory syndrome coronavirus and human coronavirus 229E mediate resistance to antiviral interferon responses. *J Gen Virol* **92**, 1899-1905 (2011).

31. K. K. Eriksson, L. Cervantes-Barragan, B. Ludewig, V. Thiel, Mouse hepatitis virus liver pathology is dependent on ADP-ribose-1"-phosphatase, a viral function conserved in the alpha-like supergroup. *J Virol* **82**, 12325-12334 (2008).

32. M. E. Grunewald *et al.*, The coronavirus macrodomain is required to prevent PARP-mediated inhibition of virus replication and enhancement of IFN expression. *PLoS Pathog* **15**, e1007756 (2019).

33. L. S. Voth *et al.*, Unique Mutations in the Murine Hepatitis Virus Macrodomain Differentially Attenuate Virus Replication, Indicating Multiple Roles for the Macrodomain in Coronavirus Replication. *J Virol* **95**, e0076621 (2021).

34. M. Dasovich *et al.*, High-Throughput Activity Assay for Screening Inhibitors of the SARS-CoV-2 Mac1 Macrodomain. *ACS Chem Biol* **17**, 17-23 (2022).

35. M. Schuller *et al.*, Fragment binding to the Nsp3 macrodomain of SARS-CoV-2 identified through crystallographic screening and computational docking. *Sci Adv* **7** (2021).

36. L. M. Sherrill *et al.*, Design, synthesis and evaluation of inhibitors of the SARS-CoV-2 nsp3 macrodomain. *Bioorg Med Chem* **67**, 116788 (2022).

37. S. T. Sowa *et al.*, A molecular toolbox for ADP-ribosyl binding proteins. *Cell Rep Methods* 10.1016/j.crmeth.2021.100121, 100121 (2021).

38. R. S. Virdi *et al.*, Discovery of Drug-Like Ligands for the Mac1 Domain of SARS-CoV-2 Nsp3. *SLAS Discov* **25**, 1162-1170 (2020).

15

609 39. G. J. Correy *et al.*, The mechanisms of catalysis and ligand binding for the SARS-CoV-2
610   NSP3 macrodomain from neutron and x-ray diffraction at room temperature. *Sci Adv* **8**,
611   eabo5083 (2022).
612 40. A. Roy *et al.*, Discovery of compounds that inhibit SARS-CoV-2 Mac1-ADP-ribose
613   binding by high-throughput screening. *Antiviral Res* **203**, 105344 (2022).
614 41. S. Gahbauer *et al.*, Iterative computational design and crystallographic screening
615   identifies potent inhibitors targeting the Nsp3 macrodomain of SARS-CoV-2. *Proc Natl
616   Acad Sci U S A* **120**, e2212931120 (2023).
617 42. I. Busnadiego *et al.*, Antiviral Activity of Type I, II, and III Interferons Counterbalances
618   ACE2 Inducibility and Restricts SARS-CoV-2. *mBio* **11** (2020).
619 43. S. Y. Liu, D. J. Sanchez, R. Aliyari, S. Lu, G. Cheng, Systematic identification of type I
620   and type II interferon-induced antiviral factors. *Proc Natl Acad Sci U S A* **109**, 4239-4244
621   (2012).
622 44. R. Channappanavar *et al.*, Dysregulated Type I Interferon and Inflammatory Monocyte-
623   Macrophage Responses Cause Lethal Pneumonia in SARS-CoV-Infected Mice. *Cell Host
624   Microbe* **19**, 181-193 (2016).
625 45. R. Channappanavar *et al.*, IFN-I response timing relative to virus replication determines
626   MERS coronavirus infection outcomes. *J Clin Invest* **129**, 3625-3639 (2019).
627 46. A. K. L. Leung, D. E. Griffin, J. Bosch, A. R. Fehr, The Conserved Macrodomain Is a
628   Potential Therapeutic Target for Coronaviruses and Alphaviruses. *Pathogens* **11** (2022).
629 47. M. L. DeDiego *et al.*, A severe acute respiratory syndrome coronavirus that lacks the E
630   gene is attenuated in vitro and in vivo. *J Virol* **81**, 1701-1713 (2007).
631 48. F. Almazan *et al.*, Engineering a replication-competent, propagation-defective Middle
632   East respiratory syndrome coronavirus as a vaccine candidate. *mBio* **4**, e00650-00613
633   (2013).
634 49. N. S. Ogando *et al.*, The Enzymatic Activity of the nsp14 Exoribonuclease Is Critical for
635   Replication of MERS-CoV and SARS-CoV-2. *J Virol* **94** (2020).
636 50. E. Kindler *et al.*, Early endonuclease-mediated evasion of RNA sensing ensures efficient
637   coronavirus replication. *PLoS Pathog* **13**, e1006195 (2017).
638 51. X. Deng *et al.*, Coronavirus nonstructural protein 15 mediates evasion of dsRNA sensors
639   and limits apoptosis in macrophages. *Proc Natl Acad Sci U S A* **114**, E4251-E4260
640   (2017).
641 52. C. E. Comar *et al.*, MERS-CoV endoribonuclease and accessory proteins jointly evade
642   host innate immunity during infection of lung and nasal epithelial cells. *Proc Natl Acad
643   Sci U S A* **119**, e2123208119 (2022).
644 53. A. K. Leung *et al.*, Poly(ADP-ribose) regulates stress responses and microRNA activity
645   in the cytoplasm. *Mol Cell* **42**, 489-499 (2011).
646 54. Y. Duan *et al.*, PARylation regulates stress granule dynamics, phase separation, and
647   neurotoxicity of disease-related RNA-binding proteins. *Cell Res* **29**, 233-247 (2019).
648 55. C. Chiale, T. T. Greene, E. I. Zuniga, Interferon induction, evasion, and paradoxical roles
649   during SARS-CoV-2 infection. *Immunol Rev* **309**, 12-24 (2022).
650 56. M. S. Abers *et al.*, Neutralizing type-I interferon autoantibodies are associated with
651   delayed viral clearance and intensive care unit admission in patients with COVID-19.
652   *Immunol Cell Biol* **99**, 917-921 (2021).

16

653 57. S. P. Smieszek, V. M. Polymeropoulos, C. Xiao, C. M. Polymeropoulos, M. H.
654   Polymeropoulos, Loss-of-function mutations in IFNAR2 in COVID-19 severe infection
655   susceptibility. *J Glob Antimicrob Resist* **26**, 239-240 (2021).
656 58. A. R. Fehr, Bacterial Artificial Chromosome-Based Lambda Red Recombination with the
657   I-SceI Homing Endonuclease for Genetic Alteration of MERS-CoV. *Methods Mol Biol*
658   **2099**, 53-68 (2020).
659 59. L. R. Wong *et al.*, Eicosanoid signalling blockade protects middle-aged mice from severe
660   COVID-19. *Nature* **605**, 146-151 (2022).
661 60. B. K. Tischer, G. A. Smith, N. Osterrieder, En passant mutagenesis: a two step
662   markerless red recombination system. *Methods Mol Biol* **634**, 421-430 (2010).
663 61. R. Channappanavar, S. Perlman, Evaluation of Activation and Inflammatory Activity of
664   Myeloid Cells During Pathogenic Human Coronavirus Infection. *Methods Mol Biol* **2099**,
665   195-204 (2020).
666
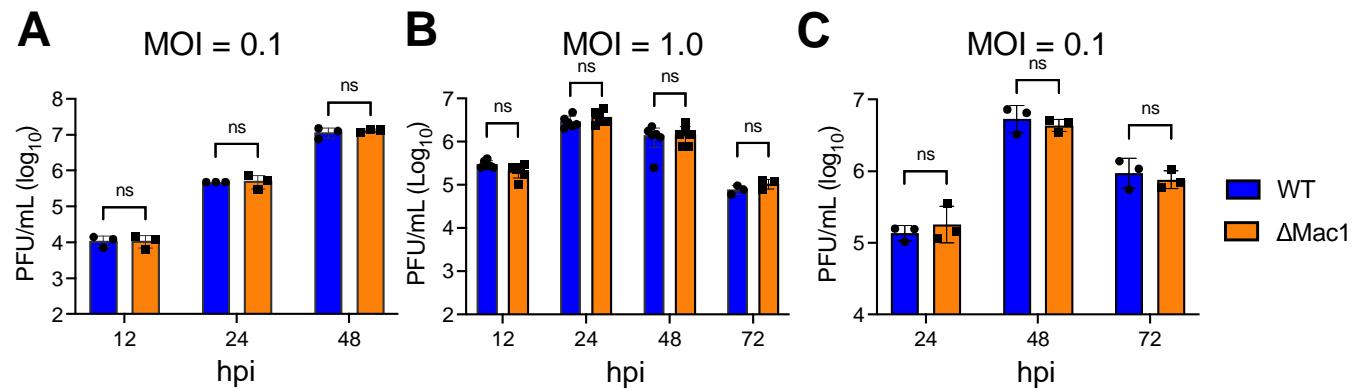
Fig. 1. SARS-CoV-2 Mac1 deletion virus replicates normally in Vero E6 and A549-ACE2 cells. VeroE6 (A-B) and A549-ACE2 (C) cells were infected with SARS-CoV-2 WT and ΔMac1 at an MOI of 0.1 (A,C) and 1 (B) PFU/cell. Both cell-associated and cell-free virus was collected at indicated time points and virus-titers were determined by plaque assays. Data shown is one experiment representative of three independent experiments. $n = 3$ per group for each experiment. ns – not significant.
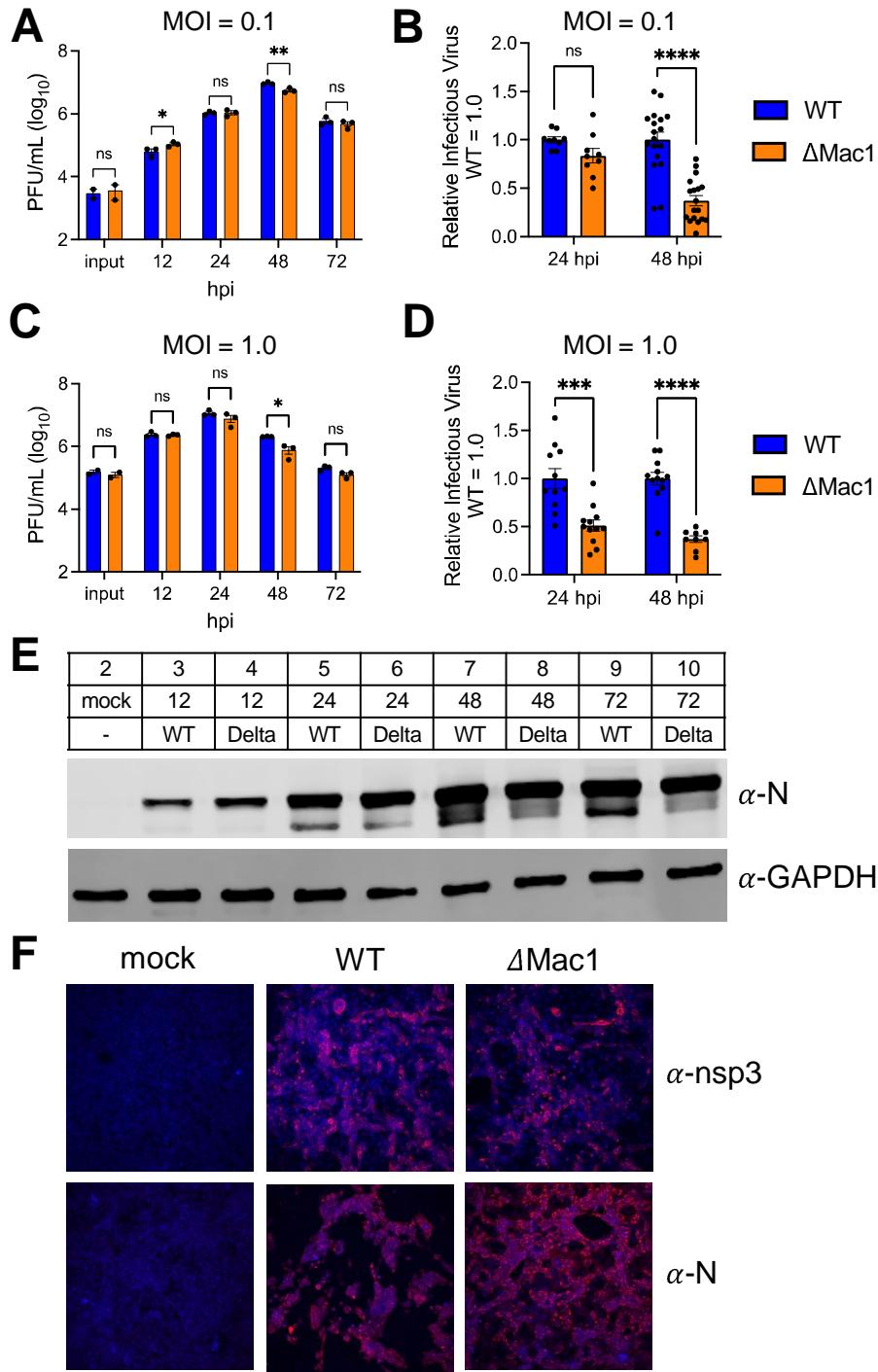
Fig. 2. SARS-CoV-2 has a mild replication defect in Calu-3 cells. (A-D) Calu-3 cells were infected with SARS-CoV-2 WT and ΔMac1 viruses at both low (A-B) and high (C-D) MOI. Both cell-associated and cell-free virus was collected at indicated times and virus titers were determined by plaque assay. The data in A & C are from one experiment representative of at least 3 independent experiments. $n = 3$ per group. The results of all combined experiments where the average WT values from each experiment were normalized to 1.0 at 24 and 48 hpi are shown in B and D. Each point represents a separate biological replicate. (E-F) Calu-3 cells were infected at an MOI of 1 PFU/cell as described above and cell lysates were collected, and viral protein levels were determined by immunoblotting (E) or cells fixed at 24 hpi were co-stained with DAPI and either anti-nsp3 or anti-N, and then analyzed by confocal microscopy at 20X magnification (F). The data in E-F shows data from one representative experiment of two independent experiments.
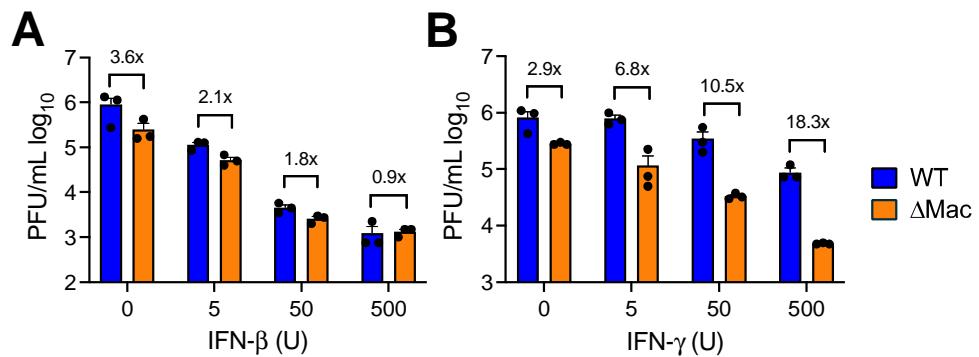
Fig. 3. IFN-γ, but not IFN-β, pretreatment enhances replication defect of ΔMac1 in Calu-3 cells. Calu-3 cells were pretreated for 18 h with increasing concentrations (0, 5, 50, and 500 units) of IFN-β (**A**) and IFN-γ (**B**), then infected with either SARS-CoV-2 WT or ΔMac1 at an MOI of 0.1 PFU/cell. Cells were collected at 48 hpi and titers were determined by plaque assay. Fold differences between WT and ΔMac1 are indicated at each amount of IFN. The data shown are of one experiment representative of two (A) and three (B) independent experiments. $n = 3$ for each group.
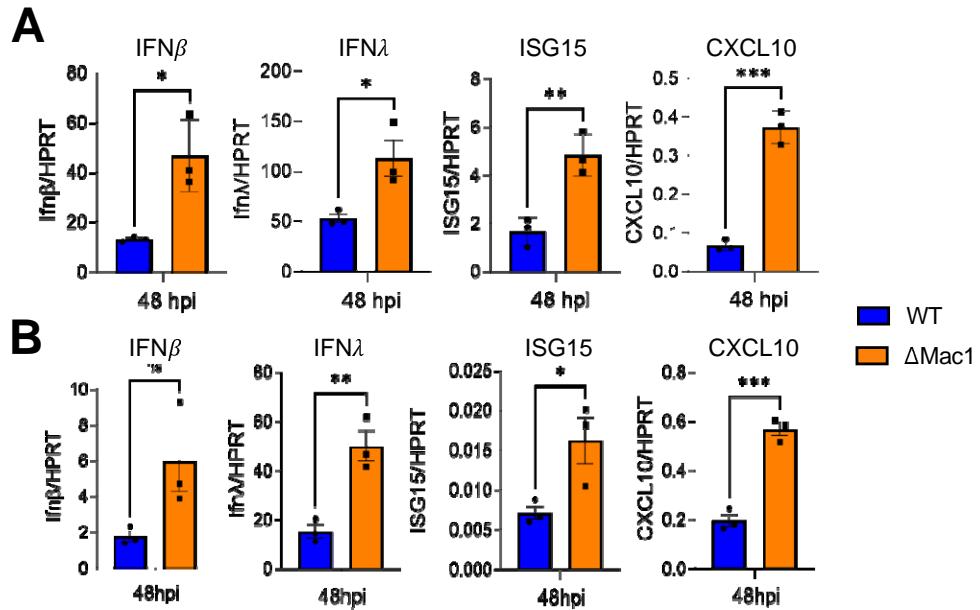
Fig. 4. *Δ*Mac1 induces increased IFN and cytokines responses compared to WT SARS-CoV-2 in cell culture. Calu3 (A) and A549-ACE2 (B) cells were infected with SARS-CoV-2 WT and ΔMac1 at an MOI of 0.1 PFU/cell and total RNA was collected 48 hpi. IFN-β, IFN-λ, ISG15 and CXCL10 levels were determined by qPCR using ΔCt method with primers listed in table S2 and normalized to HPRT mRNA levels. The data show one experimental representative of three independent experiments with $n = 3$ for each experiment.
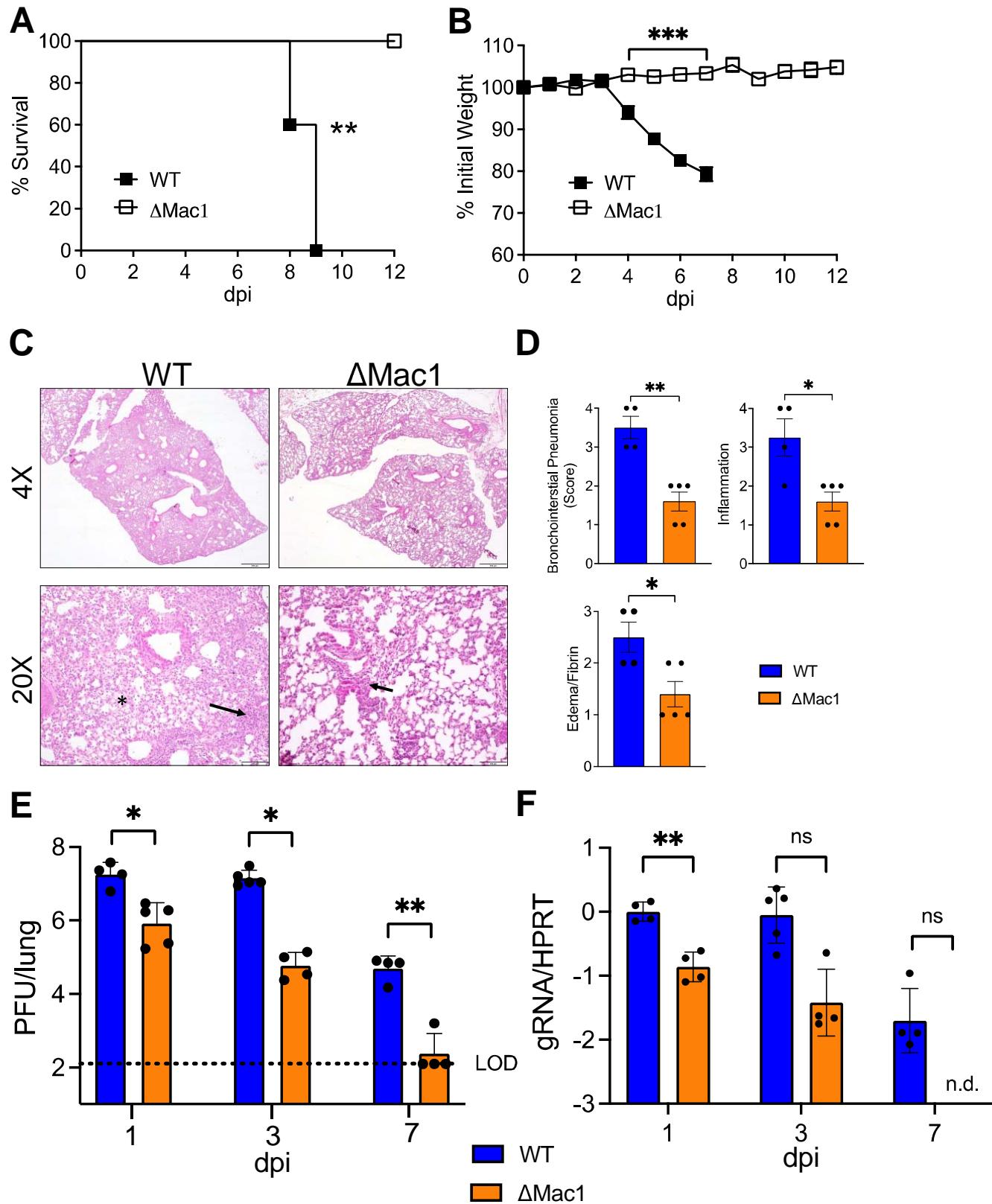
Fig. 5. *ΔMac1* is highly attenuated in K18-ACE2 mice. (A-B) K18-ACE2 C57BL/6 mice were infected with 2.5×10^4 PFU of WT or ΔMac1 SARS-CoV-2 and survival and weight loss were measured over 12 days. (C) Photomicrographs (hematoxylin and eosin stain) of lungs from WT and ΔMac1 infected mice at 7 dpi demonstrating bronchointerstitial pneumonia (black arrow) and edema and fibrin (black asterisk) (D) Mice were scored for bronchointerstitial pneumonia, inflammation, and edema/fibrin deposition. WT n=4; ΔMac1 n=5. (E-F) K18-ACE2 C57BL/6 mice were infected as described above and lung titers (E) and gRNA levels (F) were determined by plaque assay and RT-qPCR with primers specific for nsp12 and normalized to HPRT, respectively. Results are from one experiment representative of two independent experiments. *n* = 4-10 mice per group.

A

IFNβ · IFNλ2 · CXCL10 · IL6 · ISG15 · OAS3 · PARP12 · PARP14

WT (blue) · ΔMac1 (orange)

B

Number of DEG (p-adj<0.001 and FC><1.5) = 875
Genes upregulated in SARS-CoV-2ΔMac1 = 645
Genes upregulated in SARS-CoV-2 = 230

x-axis: SARS-CoV-2 WT/ΔMac1 log2FoldChange
y-axis: -log10(p-adj)

C Functional enrichment analysis

Ubl conjugation pathway · Adaptive immunity · Peptide transport · Cytolysis · Apoptosis · Inflammatory response · Antiviral defense · Innate Immunity · Immunity

P-Value
- 0.01<p<0.05
- 0.0001<p<0.01
- <0.0001

x-axis: Number of Genes

D

y-axis: SARS-CoV-2 ΔMac1/WT Log$_2$ Fold Change

Genes: Ifnl2, Ifnl3, Ifnb1, Irf7, Ifit2, Isg20, Il6, Rsad2, Oas1g, Ifit1, Apobec3, Trim30a, Bst2, Oasl1, Ifi27l2a, Mlkl, Oas3, Nt5c3, Isg15, Oas1a, Zbp1, Tgtp1, H2-Q9, Ifit3, Trex1, Stat1, Lgals9, Tlr8, Slfn8, Tlr9, Dhx58, Ifih1, Lgals8, Oas2, Cd86, Parp13, Ifitm3, Nmi, Oasl2, Pml, Samhd1, Oas1b, Ddx60, Dtx3l, Myd88, Parp9, Eif2ak2, Stat2, Itgm2, Apobec1

Fig. 6. *Δ*Mac1 virus induces a robust innate immune response in the lungs following infection. (A) K18-ACE2 C57BL/6 mice were infected with 2.5×10^4 PFU of indicated viruses and lungs were harvested at 1 dpi and total RNA was isolated. The relative levels of indicated transcripts were determined by qPCR using the ΔCt method with primers listed in table S2 normalized to HPRT mRNA levels. The results are from one experiment representative of two independent experiments with an n = 4-8 mice per group. (B-D) The total RNA from the samples in (A) were analyzed by RNAseq to determine the full transcriptome in the lung following infection. (B) Volcano plot indicating differentially expressed genes (DEGs) between WT and ΔMac1 infected mice. (C) Functional enrichment analysis of biological processes enriched in the transcriptome of in mice infected with ΔMac1 performed using DAVID functional annotation tool. (D) Log$_2$ fold change values of genes involved in innate immune response upregulated in mice infected with ΔMac1 compared to WT virus.
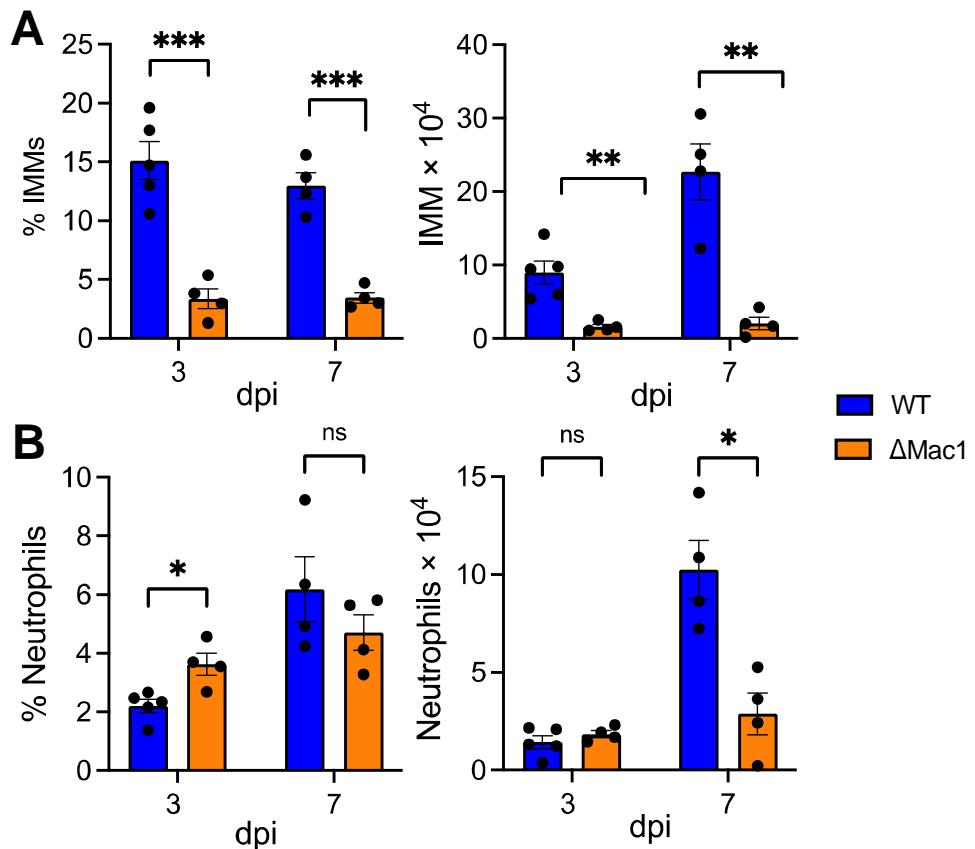
Fig. 7. *Δ*Mac1 virus infection results in reduced inflammatory monocytes and neutrophils. (A-B) K18-ACE2 C57BL/6 mice were infected as described above and lungs were harvested at the indicated days post-infection, and the percentages and total numbers of infiltrating inflammatory monocytes (A) and neutrophils (B) were determined by flow cytometry. Data are derived from the results of 1 experiment representative of 2 independent experiments performed with 4-5 mice/group/experiment.